GENETICS

Pooled CRISPR screening identifies m^{6}A as a positive regulator of macrophage activation

Jiyu Tong[1,2,3†], Xuefei Wang[1,2†], Yongbo Liu[1,2†], Xingxing Ren[4†], Anmin Wang[4], Zonggui Chen[5], Jiameng Yao[1], Kaiqiong Mao[1,2], Tingting Liu[6,7], Fei-Long Meng[6,7], Wen Pan[4], Qiang Zou[1], Jun Liu[8], Yu Zhou[5], Qiang Xia[9]*, Richard A. Flavell[10,11]*, Shu Zhu[4]*, Hua-Bing Li[1,2,9]*

m^{6}A RNA modification is implicated in multiple cellular responses. However, its function in the innate immune cells is poorly understood. Here, we identified major m^{6}A "writers" as the top candidate genes regulating macrophage activation by LPS in an RNA binding protein focused CRISPR screening. We have confirmed that *Mettl3*-deficient macrophages exhibited reduced TNF-α production upon LPS stimulation in vitro. Consistently, *Mettl3*$^{flox/flox}$; *Lyzm*-Cre mice displayed increased susceptibility to bacterial infection and showed faster tumor growth. Mechanistically, the transcripts of the *Irakm* gene encoding a negative regulator of TLR4 signaling were highly decorated by m^{6}A modification. METTL3 deficiency led to the loss of m^{6}A modification on *Irakm* mRNA and slowed down its degradation, resulting in a higher level of IRAKM, which ultimately suppressed TLR signaling–mediated macrophage activation. Our findings demonstrate a previously unknown role for METTL3-mediated m^{6}A modification in innate immune responses and implicate the m^{6}A machinery as a potential cancer immunotherapy target.

INTRODUCTION

Macrophages, serving as the first line of host defense, recognize pathogen-associated molecular patterns (PAMPs) of invading pathogens and damage-associated molecular patterns (DAMPs) from stressed or injured cells. These processes involve pattern recognition receptors (PRRs), such as Toll-like receptors (TLRs) (*1*). Depending on their genetic background and environmental stimuli, macrophages can be polarized to either an M1-like proinflammatory or tumoricidal phenotype with high capacity for antigen presentation and T cell activation or to an M2-like anti-inflammatory or protumoral phenotype with immunosuppressive function (*2*–*4*). Activated macrophages produce large numbers of chemokines and proinflammatory cytokines that attract and activate T cells to eliminate the invading pathogens. Tumor-associated macrophages (TAMs) within the tumor microenvironment represent a functional heterogeneous cell population that has a critical role in orchestrating tumor initiation and progression (*3*, *5*, *6*). Macrophage-centered strategies, including macrophage-targeting and TAM tumor-promoting blockade, began to enter clinical trials and show great potential for macrophage-based immunotherapy (*3*, *6*, *7*). Therefore, understanding the signaling involved in the activation and plasticity of TAMs will help develop better strategies for cancer immunotherapy.

The discovery of the components of the TLR signaling pathways has significantly advanced our knowledge of innate immune responses, which represent one of the most important evolutionarily conserved innate mechanisms for sensing invading pathogens. One of the most studied TLRs, TLR4, stimulates the myeloid differentiation primary response protein 88 (MyD88)- and TIR domain-containing adapter protein-inducing interferon β (TRIF)–dependent pathways, activating the transcription factor nuclear factor κB (NF-κB) and mitogen-activated protein kinases (MAPKs) and consequently inducing type I interferons and inflammatory cytokines such as tumor necrosis factor–α (TNF-α) and interleukin-6 (IL-6) (*8*, *9*). It has been demonstrated that negative regulation of the TLR signaling is strongly associated with the pathogenesis of inflammation and autoimmune diseases (*10*–*13*). We and others have shown that IL-1 receptor–associated kinase 3 (IRAK3), also known as IRAKM, is an essential negative regulator of TLR signaling pathways (*14*–*17*). The expression of IRAKM induced by the activation of macrophages prevents the dissociation of IRAK and IRAK4 from MyD88 and inhibits the formation of IRAK-TRAF6 (TNF receptor–associated factor 6) complexes. These effects of IRAKM suppress NF-κB activation and the expression of inflammatory cytokines and chemokines in macrophages, preventing the development of pathologic immune reactions (*10*, *14*). However, it remains unknown whether the posttranscriptional regulation, particularly the epigenetic modification of RNA, is involved in the control of innate immune responses in macrophages.

RNA modifications, especially the formation of N^6-methyladenosine (m^{6}A), represent one of the most delicate posttranscriptional mechanisms regulating gene expression (*18*). m^{6}A, the most abundant mRNA modification, is modulated by m^{6}A "writer," "eraser," and "reader." The m^{6}A writer complex comprises the catalytic core consisting of methyltransferase like 3 (METTL3) and methyltransferase like 14 (METTL14) and the adapter proteins Wilms tumor 1 associated

[1]Shanghai Institute of Immunology, State Key Laboratory of Oncogenes and Related Genes, Shanghai Jiao Tong University School of Medicine, Shanghai 200025, China. [2]Shanghai Jiao Tong University School of Medicine–Yale Institute for Immune Metabolism, Shanghai Jiao Tong University School of Medicine, Shanghai 200025, China. [3]Department of Pediatrics and Key Laboratory of Birth Defects and Related Diseases of Women and Children of MOE, West China Second University Hospital, Sichuan University, China. [4]Hefei National Laboratory for Physical Sciences at Microscale, the Chinese Academy of Sciences Key Laboratory of Innate Immunity and Chronic Disease, School of Basic Medical Sciences, Division of Life Sciences and Medicine, University of Science and Technology of China, 230027 Hefei, China. [5]Institute for Advanced Studies, State Key Laboratory of Virology, College of Life Sciences, Wuhan University, Wuhan 430072, China. [6]State Key Laboratory of Molecular Biology, Shanghai Institute of Biochemistry and Cell Biology, Center for Excellence in Molecular Cell Science, Chinese Academy of Sciences, Shanghai 200031, China. [7]University of Chinese Academy of Sciences, Beijing 100049, China. [8]School of Life Sciences, Peking University, Beijing 100871, China. [9]Department of Liver Surgery and State Key Laboratory of Oncogenes and Related Genes, Ren Ji Hospital, Shanghai Jiao Tong University School of Medicine, Shanghai 200127, China. [10]Department of Immunobiology, Yale University School of Medicine, New Haven, CT 06520-8055, USA. [11]Howard Hughes Medical Institute, Yale University School of Medicine, New Haven, CT 06520-8055, USA.
*Corresponding author. Email: xiaqiang@medmail.com.cn (Q.X.); zhushu@ustc.edu.cn (S.Z.); richard.flavell@yale.edu (R.A.F.); huabing.li@shsmu.edu.cn (H.-B.L.)
†These authors contributed equally to this work.

protein (WTAP), RNA binding motif protein 15 (RBM15), vir like m^{6}A methyltransferase associated (VIRMA), zinc finger CCCH-type containing 13 (ZC3H13), and Cbl proto-oncogene like 1 (CBLL1) (*19*, *20*). It has been extensively documented that m^{6}A is involved in pre-mRNA splicing, mRNA export, initiation, translation, and, predominantly, mRNA degradation (*21*, *22*). m^{6}A methylation has been regarded as a key regulator in various biological and pathological processes (*19*, *21*), but its function in the immune system has not been recognized until recently (*23*). Our previous studies demonstrated that silencing the m^{6}A methyltransferase METTL3 disrupts T cell homeostasis by targeting the IL-7/signal transducer and activator of transcription 5 (STAT5)/suppressor of cytokine signaling (SOCS) pathway and causes a systemic loss of the suppressive function of regulatory T cells (T_{regs}) (*24*, *25*). The METTL3-mediated m^{6}A modification on *Cd40*, *Cd80*, and TIR domain containing adaptor protein (*Tirap*) transcripts enhances their translation in dendritic cells, promoting dendritic cell activation (*26*). Together, these studies indicate that m^{6}A methylation plays an essential role in the maintenance of immune cell homeostasis and function. In addition, the deletion of m^{6}A demethylase alkB homolog 5, RNA demethylase (ALKBH5) in macrophages has been recently demonstrated to inhibit viral replication in vivo and in vitro (*27*, *28*). The m^{6}A reader YTH N6-methyladenosine RNA binding protein 3 (YTHDF3) suppresses interferon-dependent antiviral responses by promoting forkhead box O3 (*FOXO3*) translation (*29*). In addition, the loss of YTHDF1 in classical dendritic cells enhances the cross-presentation of tumor antigen and the cross-priming of CD8$^+$ T cells in vivo (*30*). These findings, which highlight the significance of m^{6}A modification in the immune response, prompted us to explore further the function of METTL3-mediated m^{6}A modification in macrophage activation and polarization and the role of TAMs during tumorigenesis.

Here, we have identified METTL3 as a positive regulator of the innate response of macrophages by pooled RNA binding protein (RBP) CRISPR-Cas9 screening. We have demonstrated that *Mettl3* deficiency in macrophages attenuates their ability to fight against pathogens and eliminate tumors in vivo, suggesting that METTL3-mediated m^{6}A modification is required for proper activation of macrophages. We have shown that *Mettl3* deficiency impairs the TLR4 signaling pathway in macrophages by inhibiting the degradation of *Irakm* transcripts. Thus, the present work uncovers the epitranscriptional control of the innate immune response of macrophages, providing a novel strategy to target the m^{6}A machinery for macrophage-based cancer immunotherapy.

RESULTS

Pooled CRISPR-Cas9 screen identified m^{6}A modification that promotes macrophage activation by lipopolysaccharide treatment

The posttranscriptional regulation of TLR signaling and proinflammatory cytokines is fine-controlled during macrophage activation. However, these processes have not been adequately studied. Therefore, we have investigated the posttranscriptional events in mRNA metabolism that are tightly regulated by RBPs to orchestrate fundamental cellular processes. To screen RBPs critical for macrophage activation, we prepared customized pooled RBP CRISPR-Cas9 screens. TNF-α was selected as the readout for the targeted RBP CRISPR screening since this cytokine represents the primary response during macrophage activation and can be easily detected by flow cytometry. Moreover, TNF-α has also been shown to act as a "master regulator" of inflammatory cytokine synthesis, and its aberrant production is associated with the pathogenesis of several inflammatory diseases (*31*, *32*). We have compiled and synthesized a targeted lentivirus mini-library with 7272 single guide RNAs (sgRNAs) targeting 782 genes coding for classical RBPs known in the mouse genome, as well as positive and negative controls with 10 gRNAs for each gene (listed in the Supplementary Materials). We have also generated a Raw 264.7 macrophage cell line stably expressing Cas9 and validated its functionality and effectiveness (fig. S1A). In each of the two replicate screens, 10^9 Cas9-expressing Raw 264.7 cells were infected with a lentivirus library at a multiplicity of infection (MOI) of 0.3. After selection with puromycin for 7 days, cells were stimulated with LPS and sorted on the basis of TNF-α expression (Fig. 1A and fig. S1B). sgRNAs from cells with high (TNF-α–Hi) and low (TNF-α–Low) TNF-α expression and from cells harvested on the last day of selection before sorting (presort) were amplified and sequenced. The top-ranked sgRNA enriched in TNF-α–Hi or TNF-α–Low cells showed high concordance between biological screen replicates (Fig. 1B). As expected, sgRNAs targeting known positive regulators (e.g., *Myd88* and *Irf3*) and negative regulators (e.g., *Zfp36* and *Tnfaip3*) of the LPS response were enriched in TNF-α–Low and TNF-α–Hi cells, respectively, demonstrating the success and high quality of the screens (Fig. 1C).

Besides the known regulators, we have also found that sgRNAs targeting the components of the m^{6}A writer complex—*Mettl3*, *Mettl14*, *Rbm15*, and *Nudt21*—were highly enriched in the top-ranked hits in TNF-α–Low cells. These results indicate important functions and a general role of m^{6}A modification in the activation of macrophages (Fig. 1C). To validate the involvement of m^{6}A in macrophage activation, *Mettl3* was knocked out in Raw 264.7 cells using CRISPR with new sgRNAs, and the deficiency of *Mettl3* and the substantial decrease in the overall RNA m^{6}A methylation level were confirmed (Fig. 1D). Consistent with the CRISPR screen results, the expression of TNF-α and IL-6 in *Mettl3*-depleted Raw 264.7 cells stimulated with LPS was markedly reduced in comparison to control cells (Fig. 1E and fig. S1, C to H). To further explore the biological effects of m^{6}A deficiency on macrophages, we performed RNA sequencing (RNA-seq) analysis on *Mettl3* knockout (KO) and wild-type (WT) control Raw 264.7 cells. The Gene Ontology (GO) enrichment analysis documented that the down-regulated transcripts in *Mettl3*-KO Raw 264.7 cells were enriched in innate immune response related to defense and external stimulus (Fig. 1F). Notably, in both replicates of RNA-seq, transcripts of the downstream components of the TLR4 signaling pathway, such as proinflammatory cytokines (*Tnf-α*, *Il-6*, *Il-1β*, *Il-18*, and *Il-23*) and costimulation molecules (*Cd86*), were down-regulated in *Mettl3*-deficient cells (Fig. 1G), suggesting that METTL3 has a critical function in controlling the innate immune response of Raw 264.7 macrophages.

To further confirm the biological role of the m^{6}A modification in macrophages, *Mettl3* conditional KO (CKO) mice were generated by crossing *Mettl3*$^{flox/flox}$ mice with mice expressing Cre recombinase under the control of lysozyme 2 promoter (*Lyzm*-Cre). We have documented the loss of both the METTL3 protein and the overall m^{6}A modification in bone marrow–derived macrophages (BMDMs) from *Mettl3*$^{flox/flox}$;*Lyzm*-Cre mice (fig. S1I). No differences in the frequency of major immune cell populations were observed between *Mettl3*$^{flox/flox}$ mice and *Mettl3*$^{flox/flox}$;*Lyzm*-Cre mice in steady state, indicating that the depletion of *Mettl3* did not affect the development and maturation of macrophages (fig. S1J). Next, we examined whether METTL3 affects macrophage activation.

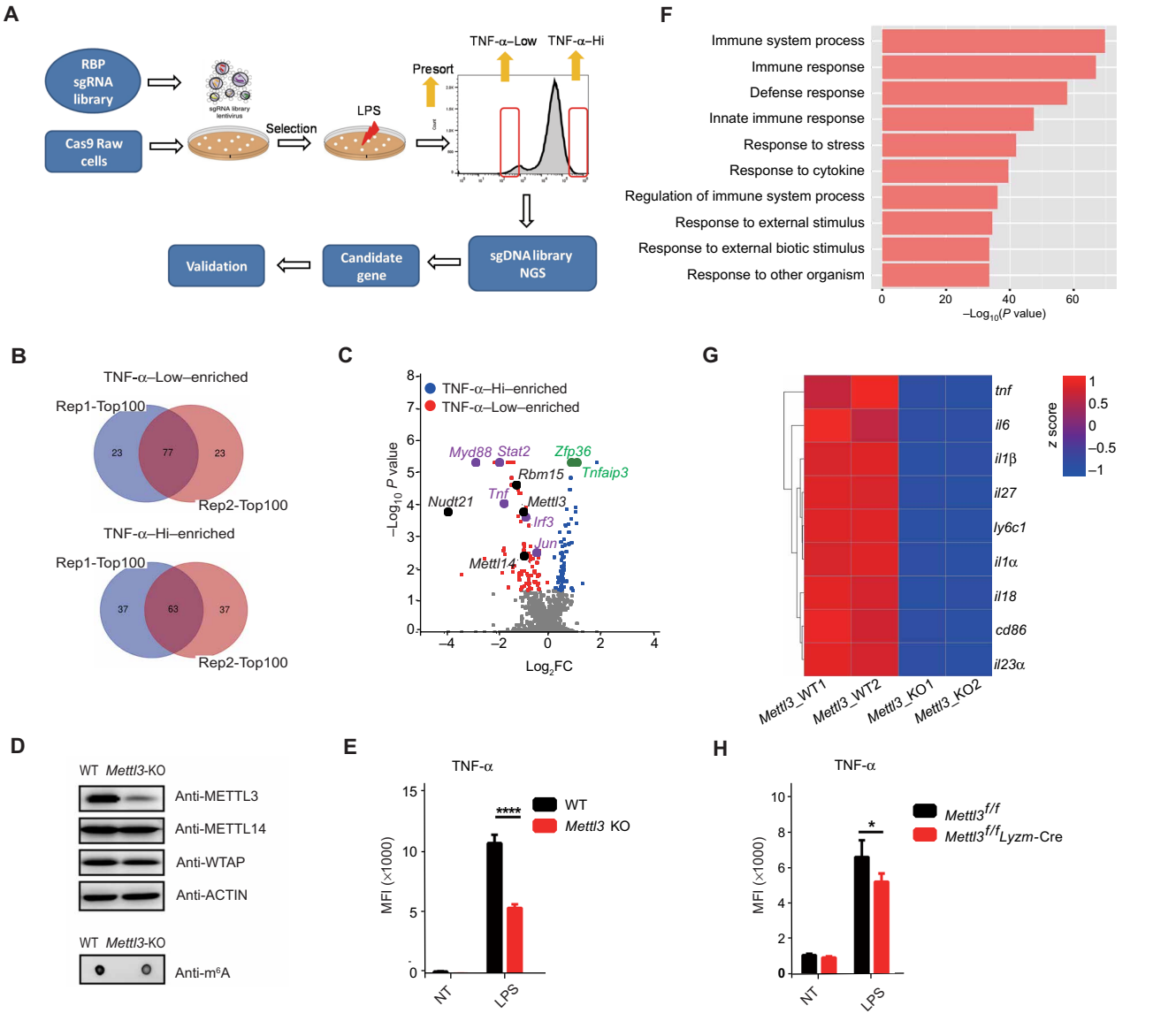

Fig. 1. CRISPR screening identifies METTL3 as a regulator of TNF-α production in macrophages. (**A**) Scheme of pooled CRISPR-Cas9 screening of RBPs playing critical roles in macrophage activation. Briefly, Cas9-expressing Raw 264.7 cells were infected with lentivirus library containing sgRNAs targeting RBP genes in the mouse genome. After selection with puromycin for 7 days, the cells were stimulated with LPS and sorted by flow cytometry on the basis of the expression levels of TNF-α. (**B**) Venn diagrams showing the overlap between the top 100 ranked candidate genes enriched in TNF-α–Low and TNF-α–Hi populations in two replicate screens. (**C**) Volcano plot showing sgRNA-targeted genes enriched in the TNF-α–Hi (blue) and TNF-α–Low (red) populations. Known positive regulators (purple), negative regulators (green), and m^{6}A modulators (black) of TNF-α production in macrophages are highlighted. (**D**) Protein level of METTL3 and the overall RNA m^{6}A methylation levels in WT and *Mettl3*-KO Raw 264.7 cells were measured by Western blotting and m^{6}A dot blot assay. (**E**) Expression of TNF-α in METTL3-depleted and control Raw 264.7 cells after LPS stimulation measured by flow cytometry. MFI, median fluorescence intensity; NT, not treated. (**F**) GO enrichment analysis of down-regulated transcripts in *Mettl3*-KO Raw 264.7 cells compared to WT control cells. (**G**) Heatmap illustrating the expression of transcripts downstream of the TLR4 signaling pathway in *Mettl3*-deficient and WT Raw 264.7 cells. (**H**) Expression of TNF-α in bone marrow–derived macrophages (BMDMs) from *Mettl3*$^{flox/flox}$;*Lyzm*-Cre and *Mettl3*$^{flox/flox}$ control mice upon LPS stimulation measured by flow cytometry. Data are shown from two experiments (B and C), as a representative result of three independent experiments (D), or as means ± SEM (E and H).*$P < 0.05$ and ****$P < 0.0001$ (unpaired two-tailed Student's *t* test).

Consistent with the results obtained in Raw 264.7 cells, BMDMs from *Mettl3*$^{flox/flox}$;*Lyzm*-Cre mice showed significantly decreased expression of proinflammatory cytokines, such as TNF-α, IL-6, IL-1β, and IL-12, upon LPS stimulation (Fig. 1H and fig. S1K). Together, these results demonstrate that METTL3 promotes the activation of macrophages.

Notably, the m^{6}A readers, including YTHDF1, YTHDF2, YTHDF3, YTHDC1, YTHDC2, IGF2BP1, IGF2BP2, IGF2BP3, HNRNPC, and HNRNPA2B1, did not reach significance in either TNF-α–Low or TNF-α–High population (fig. S2A and table S1), indicating that these genes either play a minimal role or have redundant functions in regulating the LPS-induced *Tnf*-α production. To further assess the

functional role of m^{6}A readers in macrophages, small interfering RNAs (siRNAs) were used to knock down the expression of *Ythdf2* and other readers, including *Ythdf1*, *Ythdf3*, and *Ythdc1* in bone marrow derived macrophages (BMDMs) (fig. S2B). As shown in fig. S2C, we found that knocking down *Ythdf2*, *Ythdf3*, or *Ythdc1* individually had a minor impact on *Tnf*-α expression upon LPS stimulation, whereas knocking down *Ythdf1* decreased the expression of *Tnf*-α, and markedly higher down-regulation of *Tnf-α* was seen when knocking down the expression of *Ythdf1*, *Ythdf2*, and *Ythdf3* simultaneously. These results suggested the functional redundancy of YTHDF proteins in the innate immune response of macrophages (*33*, *34*). In addition to the involvement of m^{6}A modification in the activation of macrophages by LPS, other pathways associated with the mRNA metabolic process have also been found by GO and Kyoto Encyclopedia of Genes and Genomes (KEGG) analyses of the top 100 ranked hits in TNF-α–Hi and TNF-α–Low cells (fig. S2, D to G), which merits further exploration.

Mettl3-deficient mice are more susceptible to *Salmonella typhimurium* infection

Upon recognizing invading pathogens, macrophages are activated to produce proinflammatory cytokines, such as TNF-α and IL-6, that enhance the defense response of the host, facilitating pathogen clearance. To test the screen results in vivo, we investigated the physiological role of m^{6}A modification in the macrophage-mediated defense against LPS-producing Gram-negative bacteria. For this purpose, *Mettl3*$^{flox/flox}$; *Lyzm*-Cre mice and *Mettl3*$^{flox/flox}$ littermates were infected orally with *S. typhimurium* and sacrificed 4 days after infection to assess the inflammation and bacterial load in the intestine and other organs. *Mettl3*$^{flox/flox}$;*Lyzm*-Cre mice showed significantly lower body weight than *Mettl3*$^{flox/flox}$ littermates (Fig. 2A) and had a higher bacterial load in the feces and cecum (Fig. 2, B to D). Furthermore, *Mettl3*$^{flox/flox}$; *Lyzm*-Cre mice had a higher bacterial burden in the spleen and liver than *Mettl3*$^{flox/flox}$ littermates (Fig. 2, E and F). Together, these data suggest that METTL3 promotes the antibacterial activity of macrophages in vivo.

Loss of METTL3 in macrophages promotes tumor growth in vivo

Given the function of m^{6}A in promoting macrophage activation, we next sought to determine the role of METTL3 in macrophage-mediated antitumor immunity. Therefore, MC38 murine colon adenocarcinoma cells were subcutaneously implanted into the flanks of *Mettl3*$^{flox/flox}$; *Lyzm*-Cre mice and their *Mettl3*$^{flox/flox}$ littermates. The growth of tumors was significantly faster in *Mettl3*$^{flox/flox}$;*Lyzm*-Cre mice (Fig. 3, A and B, and fig. S3A). The mice were sacrificed 3 weeks

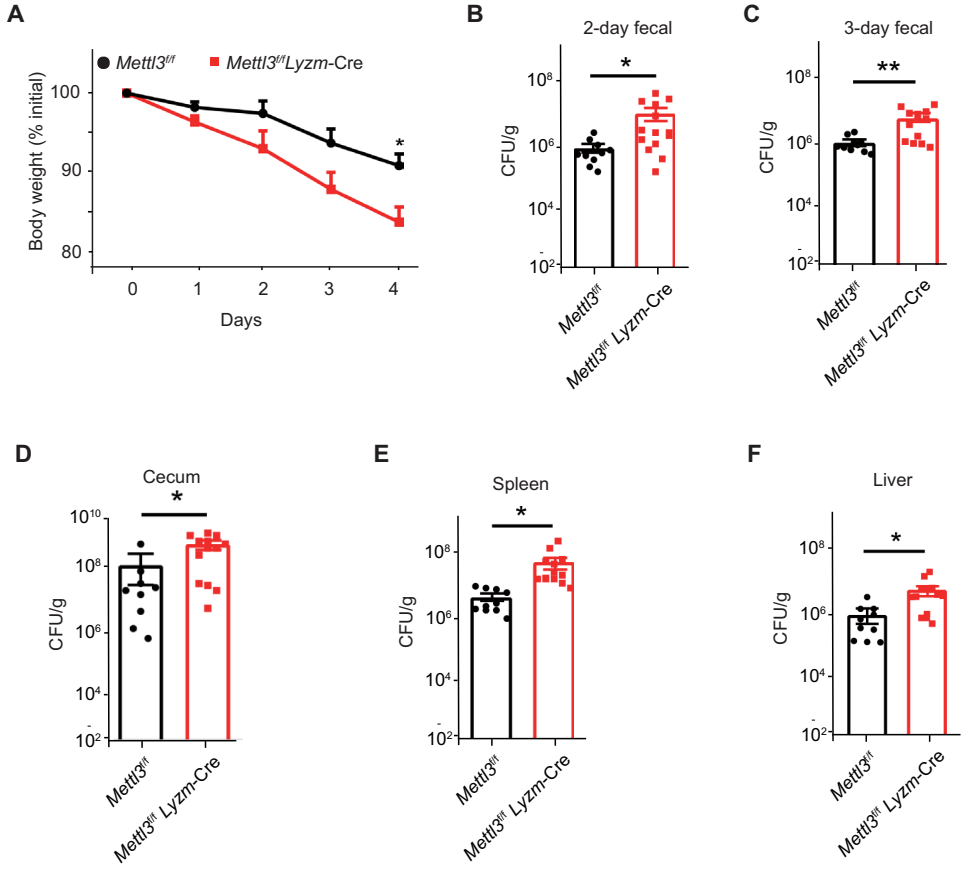

Fig. 2. *Mettl3*$^{flox/flox}$;*Lyzm*-Cre mice are more susceptible to *S. typhimurium* infection. (**A**) Body weight of *Mettl3*$^{flox/flox}$;*Lyzm*-Cre ($n = 14$) and their *Mettl3*$^{flox/flox}$ littermates ($n = 10$) measured 2 and 3 days after *S. typhimurium* infection. (**B** to **F**) Bacteria load of the feces (B and C), cecum (D), spleen (E), and liver (F) of infected *Mettl3*$^{flox/flox}$;*Lyzm*-Cre ($n = 14$) and *Mettl3*$^{flox/flox}$ littermates ($n = 10$) measured by counting colony-forming units (CFU) in cultures of serially diluted homogenates of organs on MacConkey agar plates. Data are shown as representative results of three independent experiments (A to F) or as means ± SD of indicated determinants (B to F). *$P < 0.05$ and **$P < 0.01$ (unpaired two-tailed Student's *t* test).

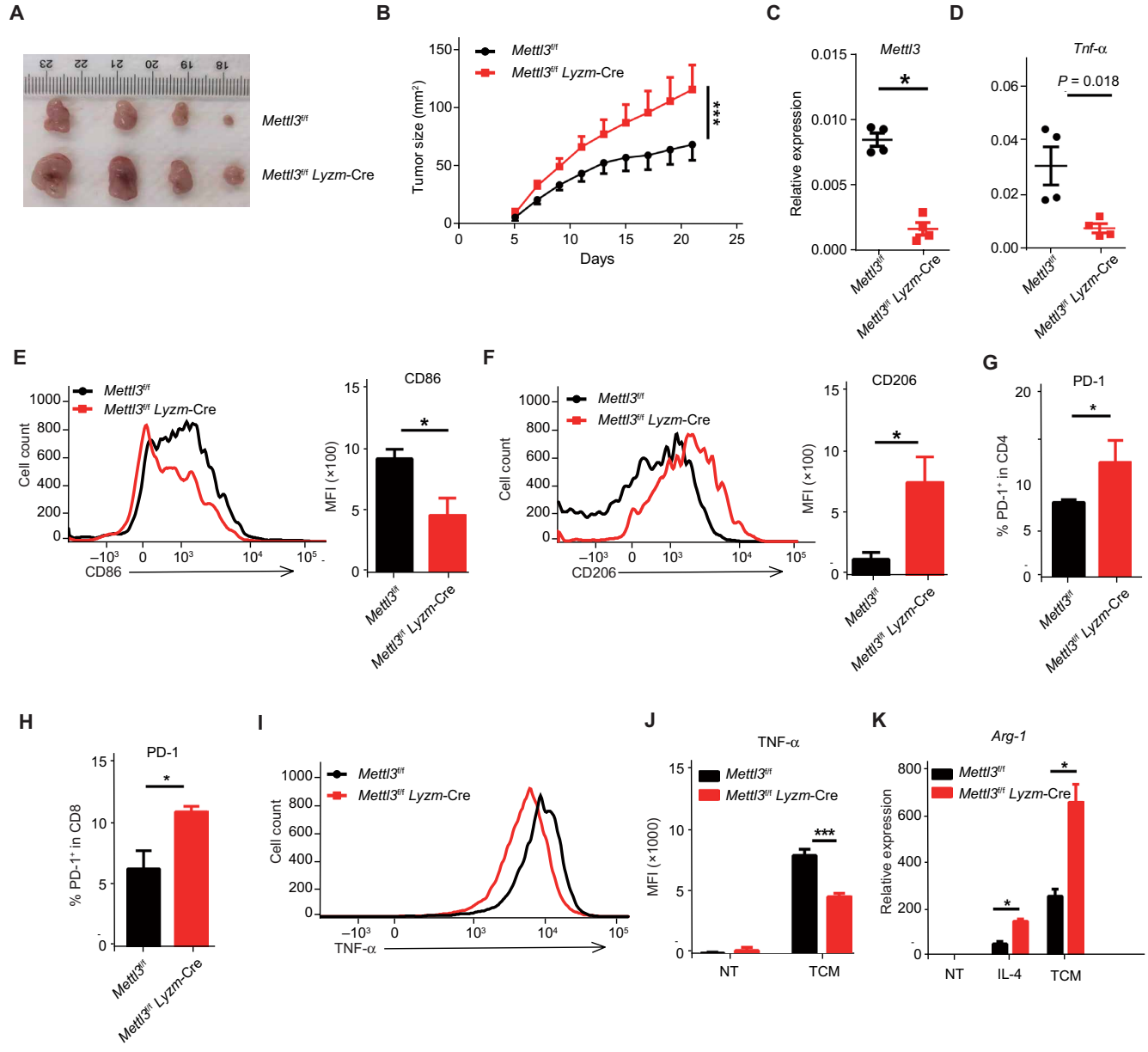

Fig. 3. *Mettl3*$^{flox/flox}$;*Lyzm*-Cre mice exhibit faster tumor growth and a lower level of macrophage-derived TNF-α than WT littermates. MC38 cells were subcutaneously injected into the flanks of *Mettl3*$^{flox/flox}$;*Lyzm*-Cre mice and their *Mettl3*$^{flox/flox}$ littermates. The tumor was excised, and tumor-infiltrating cells were characterized by flow cytometry and real-time qPCR. (**A**) Representative images of tumors excised from *Mettl3*$^{flox/flox}$;*Lyzm*-Cre mice ($n = 10$) and *Mettl3*$^{flox/flox}$ littermates ($n = 10$) 21 days after cell injection. Photo credit: Jiyu Tong, Shanghai Jiao Tong University School of Medicine. (**B**) Tumor growth in *Mettl3*$^{flox/flox}$;*Lyzm*-Cre mice ($n = 10$) and *Mettl3*$^{flox/flox}$ littermates ($n = 10$). (**C** and **D**) Relative expression of *Mettl3* (C) and *Tnf-α* (D) in TAMs from *Mettl3*$^{flox/flox}$;*Lyzm*-Cre mice ($n = 4$) and *Mettl3*$^{flox/flox}$ littermates ($n = 4$) measured by real-time qPCR. (**E** and **F**) Flow cytometry profile and MFI of CD86-positive (E) and CD206-positive (F) TAMs from *Mettl3*$^{flox/flox}$;*Lyzm*-Cre mice ($n = 4$) and *Mettl3*$^{flox/flox}$ littermates ($n = 4$). (**G** and **H**) Fractions of intratumoral PD-1–positive CD4$^+$ T cells (G) and PD-1–positive CD8$^+$ T cells (H) measured by flow cytometry ($n = 3$). (**I** and **J**) BMDMs from *Mettl3*$^{flox/flox}$;*Lyzm*-Cre mice and *Mettl3*$^{flox/flox}$ littermates were stimulated with medium conditioned by MC38 tumor cells in vitro. The expression of TNF-α was measured by flow cytometry and shown as a histogram (I) and MFI (J). *Arg-1* expression in TAMs from *Mettl3*$^{flox/flox}$;*Lyzm*-Cre mice and *Mettl3*$^{flox/flox}$ littermates measured by real-time qPCR after TCM or IL-4 treatment. Data are shown as representative results of three independent experiments (A, E, F, and I), as means ± SD (B, G, and H), or as means ± SEM (C to F, J, and K). *$P < 0.05$ and ***$P < 0.001$ (unpaired two-tailed Student's *t* test).

after injection, and tumor-infiltrating immune cells were characterized by flow cytometry and real-time quantitative polymerase chain reaction (qPCR). There was no significant difference in the percentage of tumor-infiltrating lymphocytes between *Mettl3*$^{flox/flox}$;*Lyzm*-Cre mice and *Mettl3*$^{flox/flox}$ littermates (fig. S3B). Notably, TAMs from *Mettl3*$^{flox/flox}$;*Lyzm*-Cre mice exhibited reduced M1-like markers, such as the proinflammatory cytokine TNF-α and the costimulatory protein CD86 (Fig. 3, C to E, and fig. S3C), while the expression of the mannose receptor CD206, a well-established M2-like marker, was increased in comparison with TAMs from *Mettl3*$^{flox/flox}$ mice (Fig. 3F and fig. S3C). These differences indicate that *Mettl3* deficiency promotes the immunosuppressive function of TAMs. In addition,

the expression of major histocompatibility complex II (MHC II) was comparable in TAMs from *Mettl3*$^{flox/flox}$;*Lyzm*-Cre mice and *Mettl3*$^{flox/flox}$ littermates (fig. S3C). Consistent with these observations, both tumor-infiltrating CD4$^+$ and CD8$^+$ T cells from *Mettl3*$^{flox/flox}$;*Lyzm*-Cre mice displayed a more exhausted phenotype, as evidenced by the elevated expression of the immune checkpoint receptor programmed cell death 1 (PD-1) (Fig. 3, G and H, and fig. S3D). Furthermore, in comparison with *Mettl3*$^{flox/flox}$ mice, BMDMs from *Mettl3*$^{flox/flox;}$*Lyzm*-Cre mice were characterized by blunted TNF-α production after the stimulation with MC38 tumor culture medium (TCM) (Fig. 3, I and J) and increased formation of the M2-like marker Arg-1 after either TCM or IL-4 stimulation (Fig. 3K and fig. S3E). Collectively, these data demonstrate that METTL3 promotes the tumoricidal ability of macrophages by facilitating the polarization bias of TAMs toward the M1 type macrophages.

METTL3 deficiency inhibits macrophage activation by inducing a negative regulator of the TLR signaling pathway

To distinguish whether macrophage activation was impeded by the disruption of m^{6}A modification rather than an m^{6}A-independent activity of METTL3, we performed rescue experiments by overexpressing WT METTL3 (METTL3-WT) or catalytic mutant METTL3 (METTL3-MUT) in BMDMs from *Mettl3*$^{flox/flox}$;*Lyzm*-Cre mice and *Mettl3*$^{flox/flox}$ littermate controls. The expression of TNF-α in BMDMs from *Mettl3*$^{flox/flox}$;*Lyzm*-Cre animals could only be restored by the *Mettl3*-WT, but not *Mettl3*-MUT constructs (fig. S4A). Since *Tnf*-α mRNA can also be m^{6}A-modified according to the m^{6}AVar database, we hypothesized that *Tnf*-α might be directly regulated by m^{6}A. First, the degradation rate of *Tnf*-α mRNAs was measured using RNA decay assays. Both *Mettl3*-depleted and WT Raw 264.7 cells were treated with the transcription inhibitor actinomycin D, and the changes in the abundance of *Tnf*-α transcripts over time were measured by qPCR. The degradation of *Tnf*-α mRNAs was similar in *Mettl3*-depleted Raw 264.7 cells and WT control cells (fig. S4B). Next, a mutagenesis assay was performed to directly assess the effect of m^{6}A modification on TNF-α expression. The assay used a WT *Tnf*-α construct in which WT *Tnf*-α 5′ untranslated region (5′UTR) and WT *Tnf*-α 3′UTR were replaced with either *Tnf*-α 5′UTR-MUT or *Tnf*-α 3′UTR-MUT harboring a point mutation in m^{6}A sites predicted according to the m^{6}AVar database (fig. S4C). The coding region of *Tnf*-α was substituted with a green fluorescent protein (GFP) coding region to allow direct measurement of TNF-α expression. A similar level of GFP expression was observed when human embryonic kidney (HEK) 293 cells were transfected with the same amount of each construct (fig. S4D). Therefore, these experiments demonstrated that although macrophage activation was indeed regulated by the m^{6}A catalytic activity of METTL3, *Tnf*-α mRNA was not the direct target of the m^{6}A modification.

It is well established that the engagement of PAMPs or DAMPs with TLR4 receptors activates MyD88- and TRIF-dependent pathways and ultimately induces the synthesis of proinflammatory cytokines required for pathogen clearance or the destruction of tumor cells (*6*, *35*). Since a defective expression of a broad range of cytokines was observed (Fig. 1G and fig. S1K), we hypothesized that the TLR4 receptor and its downstream pathway were compromised in *Mettl3*-deficient macrophages and could represent the direct m^{6}A targets. Upon LPS stimulation, the phosphorylation of p65, p38, c-Jun N-terminal kinase (JNK), and extracellular signal–regulated kinase (ERK) in *Mettl3*-deficient BMDMs was markedly decreased, but the total levels of these proteins were comparable between BMDMs from *Mettl3*$^{flox/flox}$;*Lyzm*-Cre mice and their *Mettl3*$^{flox/flox}$ littermates (Fig. 4A). These data indicate that the *Mettl3* deficiency probably affects molecules upstream of the NF-κB and mitogen-activated protein kinase (MAPKs) pathways. Therefore, we examined the expression levels of essential upstream adaptors in the TLR4 pathway, including *Tirap*, *Myd88*, *Traf6*, *Irak1*, *Irak4*, *Trif*, and *Tram*, using real-time qPCR. The expression of these key adaptors was similar in WT and *Mettl3*-deficient BMDMs (Fig. 4B). However, we have noted that the mRNA and protein levels of *Irakm*, a well-established negative regulator of the TLR signaling pathway, were remarkably increased in *Mettl3*-deficient BMDMs in either steady-state or upon LPS stimulation (Fig. 4, A and C). The expression of IRAKM in WT macrophages was reduced immediately after LPS stimulation and began to recover 2 hours after TLR4 activation. This phenomenon was strongly inhibited in *Mettl3*-KO macrophages, resulting in a sustained overexpression of IRAKM (Fig. 4A and fig. S4E). Thus, we have raised the possibility that the overexpression of IRAKM caused by *Mettl3* deficiency is responsible for the inhibition of TLR4 activation. To test this hypothesis, rescue experiments were performed by introducing either *Irakm* small hairpin RNA (shRNAs) (sh-*Irakm*) or control shRNAs (sh-*CTL*) into *Mettl3*-deficient BMDMs (Fig. 4D). Consistent with our prediction, the decrease in TNF-α production in *Mettl3*-deficient BMDMs was largely reversed by the shRNA-mediated knockdown of *Irakm* (Fig. 4E). Together, these data indicate that the overexpression of *Irakm* in *Mettl3*-deficient macrophages suppresses the TLR4 signaling and consequently inhibits macrophage activation.

In addition, we tested other TLR pathways known to be regulated through IRAKM, especially TLR3 and TLR9. Similarly, TNF-α production of BMDMs from *Mettl3*$^{flox/flox}$; *Lyzm-Cre* mice was significantly decreased upon poly (I:C) or CpG stimulation (fig. S5A and S5B). Thus, m^{6}A regulates TLR-mediated macrophage activation through *Irakm*.

METTL3 installs m^{6}A modifications on *Irakm* mRNA, promoting its degradation

RNA m^{6}A methylation is involved in multiple aspects of RNA metabolism (*36*), predominantly affecting RNA stability. *Mettl3* deficiency results in a significantly decreased m^{6}A marker and, in turn, retards RNA decay of m^{6}A target transcripts (*37*, *38*). To assess whether the deletion of *Mettl3* can decrease m^{6}A methylation of *Irakm* mRNA, we profiled the transcriptome-wide m^{6}A modification in WT and *Mettl3*-deficient Raw 264.7 cells using m^{6}A immunoprecipitation followed by high-throughput sequencing (MeRIP-seq). Specific m^{6}A peaks were clearly enriched in the 3′UTR of *Irakm* mRNAs in WT cells, but the deletion of *Mettl3* eliminated the *Irakm* m^{6}A peaks completely (Fig. 5A). Notably, we did not detect significant m^{6}A peak reduction in the *Tnf*-α transcript (fig. S6A) and did not observe any significant m^{6}A peaks throughout *Il-6* transcript (fig. S6B), indicating that *Tnf*-α and *Il-6* are not direct m^{6}A targets in macrophages. In agreement with the sequencing data, MeRIP-qPCR demonstrated that *Irakm* mRNA from WT but not *Mettl3*-deficient macrophages was immunoprecipitated by m^{6}A-specific antibody (Fig. 5B). Together, these findings document that *Irakm* transcripts are bona fide m^{6}A targets in macrophages.

To further test whether the up-regulation of IRAKM resulted from the decreased degradation of m^{6}A-deficient *Irakm* transcripts, we have performed RNA decay assays by treating either WT or *Mettl3*-deficient BMDMs and Raw 264.7 cells with actinomycin D and

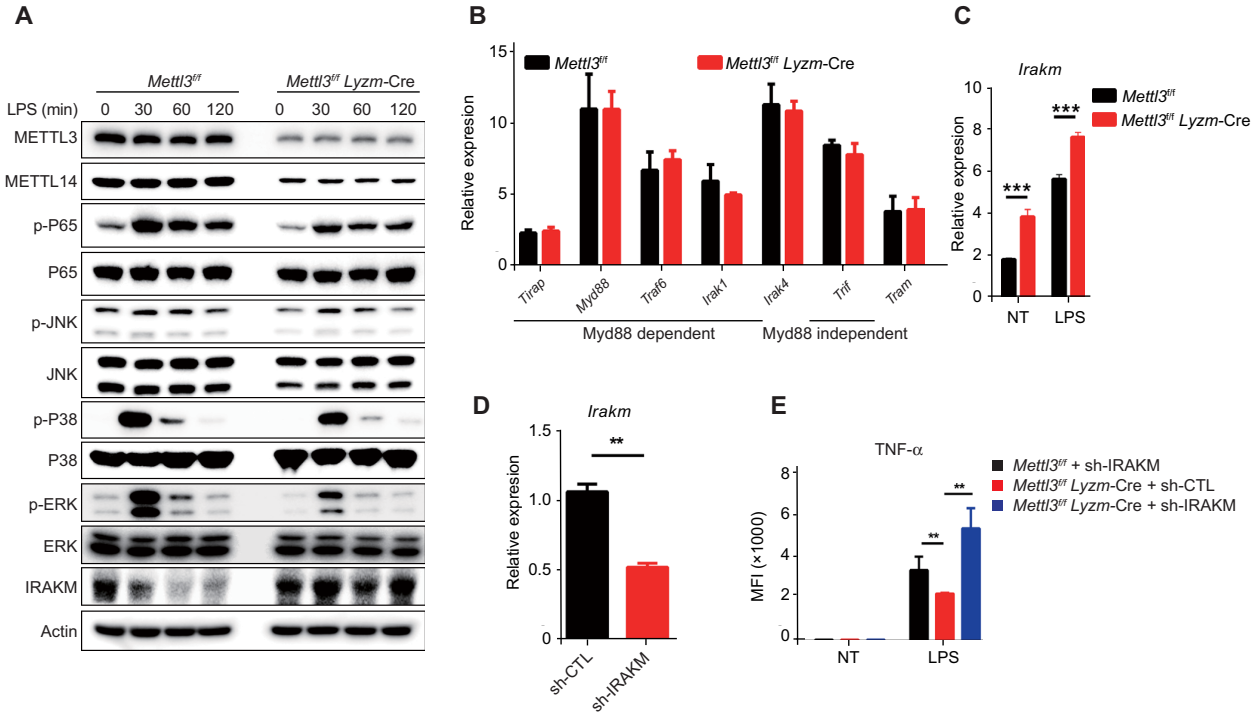

Fig. 4. METTL3 deficiency impairs the TLR4 signaling pathway by modulating IRAKM expression. (**A**) Activation of the TLR4 signaling pathway in *Mettl3*-KO and *Mettl3*-WT BMDMs upon LPS stimulation was analyzed by Western blotting of p65, JNK, p38, ERK, and IRAKM. (**B**) Relative expression of *Tirap*, *Myd88*, *Traf6*, *Irak*, *Irak4*, *Trif*, and *Tram* in *Mettl3*$^{flox/flox}$;*Lyzm*-Cre mice and *Mettl3*$^{flox/flox}$ littermates measured by real-time qPCR. (**C**) Relative expression of *Irakm* in control (NT) and LPS-treated *Mettl3*$^{flox/flox}$;*Lyzm*-Cre and *Mettl3*$^{flox/flox}$ littermates measured by real-time qPCR. (**D**) Knockdown efficiency of shRNA targeting *Irakm* in BMDMs measured by real-time qPCR ($n = 3$). (**E**) TNF-α synthesis in WT BMDMs transfected with control shRNA (sh-CTL) and *Mettl3*-deficient BMDMs transfected with sh-CTL or IRAKM shRNA (sh-IRAKM) measured by flow cytometry ($n = 3$). Data are shown as representative results of three independent experiments (A) or as means ± SEM (B to E). $^{**}P < 0.01$ and $^{***}P < 0.001$ (unpaired two-tailed Student's *t* test).

measured the abundance of *Irakm* transcripts over time (Fig. 5C and fig. S6C). At 3 hours after actinomycin D treatment, *Irakm* mRNA level was significantly higher in *Mettl3*-deficient BMDMs and Raw 264.7 cells than in the WT control cells (Fig. 5C and fig. S6C). To directly evaluate the role of m^{6}A in modulating the stability of *Irakm* mRNA, luciferase reporter assays were conducted. In comparison with WT *Irakm*-3′UTR (*Irakm*-WT) constructs, the ectopically expressed constructs harboring m^{6}A mutant *Irakm*-3′UTR (*Irakm*-MUT) showed substantially increased luciferase activity (Fig. 5D). We also constructed a plasmid harboring IRAKM with either WT-3′UTR or m^{6}A–mut-3′UTR. Consistent with our previous results, we found that the transcription level of *Irakm* with m^{6}A–mut-3′UTR was notably higher than that of *Irakm* with WT 3′UTR (fig. S6D). In addition, we also tested the effect of METTL3 deficiency on transcription of *Irakm* mRNA. As shown in the fig. S6E, we found that the transcription rate of *Irakm* mRNA only slightly increased upon *Mettl3* KO. Therefore, the effect of METTL3 deficiency on *Irakm* expression was a combination of both transcription and decay but mainly due to decelerated degradation of *Irakm* mRNAs. Collectively, these data demonstrate that METTL3-mediated m^{6}A modification promotes the TLR4 signaling mainly by accelerating the degradation of *Irakm* mRNAs.

A novel mechanism has recently been revealed by which m^{6}A methylation facilitates the decay of the chromosome-associated regulatory RNAs (carRNAs), including promoter-associated RNAs (paRNAs), enhancer RNAs (eRNAs), and repeat RNAs, affecting local chromatin state and downstream transcription (*39*). To assess the potential function of *Mettl3* on chromatin openness and nascent transcripts synthesis in BMDMs, we performed deoxyribonuclease I (DNase I)–terminal deoxynucleotidyl transferase–mediated deoxyuridine triphosphate nick end labeling (TUNEL) and 5-ethynyl uridine (EU) labeling assays in BMDMs from *Mettl3*$^{flox/flox}$ and *Mettl3*$^{flox/flox}$;*Lyzm*-Cre mice (fig. S7, A and B). Similar chromatin accessibility and nascent transcripts synthesis were observed between WT and *Mettl3*-deficient BMDMs (fig. S7, A and B). Furthermore, by analyzing the m^{6}A-modified carRNAs in macrophages based on our MeRIP-seq data, we did not identify any significant m^{6}A peaks on paRNA and eRNA upstream of *Tnf*-α and *Irakm* (fig. S7, C and D), under the conditions that successfully called significant m^{6}A-marked carRNAs for genes such as *Vars* (fig. S8A). In addition, no significant carRNAs were identified in BMDMs for TLR-related genes, including TRIAP, MyD88, TRAF6, IRAK4, and TRAM (fig. S8, B to E). Further, although carRNAs of *Irakm* were observed in mouse embryonic stem cells (mESCs) (table S4), no significant *Irakm* carRNAs were identified in BMDMs of our MeRIP-seq data. In addition, our MeRIP-qPCR results showed that the levels of *Irakm* carRNAs were largely unchanged with knockout of METTL3 in BMDMs, except for a slight decrease in *Irakm* eRNA(+), which may account for the slightly increased transcription of *Irakm* in METTL3-KO BMDMs. Therefore, in contrast to the findings in mESCs, our results demonstrated that in macrophages, m^{6}A regulates TNF-α production by targeting the degradation of *Irakm* mRNA.

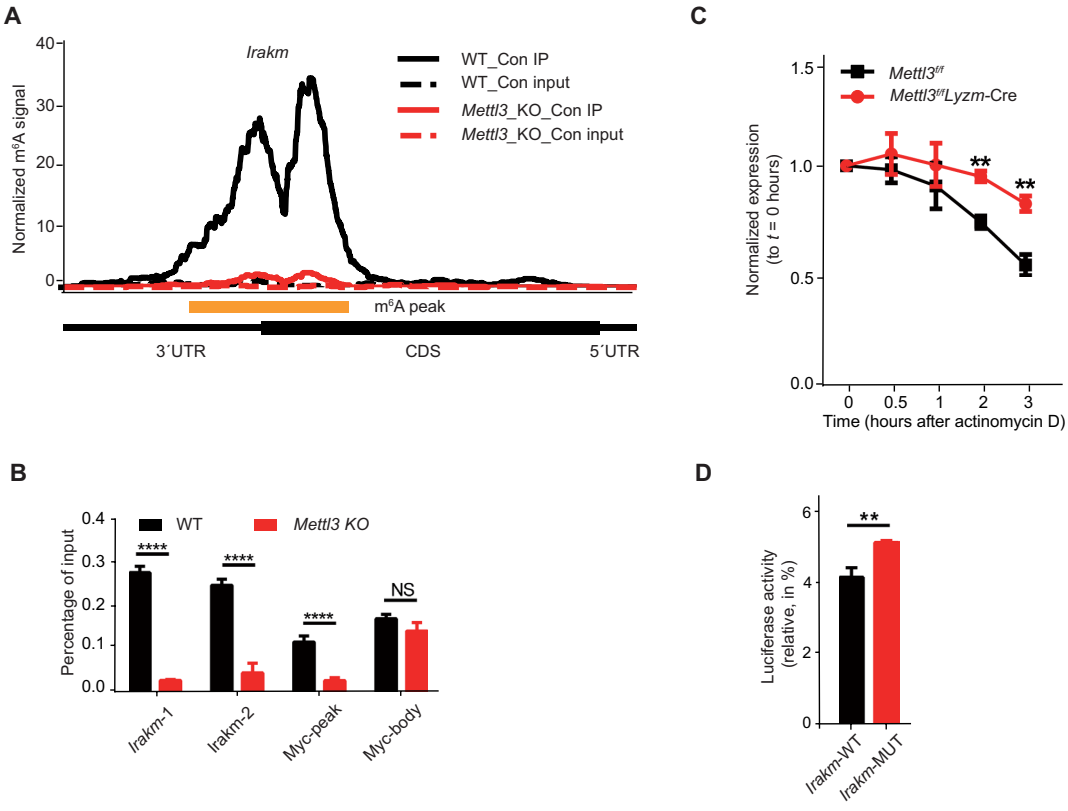

Fig. 5. IRAKM expression is down-regulated by m^{6}A modification. (**A**) Specific m^{6}A peaks enriched in the 3′UTR of *Irakm* mRNAs in Raw 264.7 macrophages profiled using MeRIP-seq. CDS, coding sequences. (**B**) m^{6}A peaks enriched in the 3′UTR of *Irakm* mRNAs in WT cells were lost in *Mettl3*-KO Raw 264.7 cells. (**C**) WT or *Mettl3*-deficient BMDMs were treated with the transcription inhibitor actinomycin D, and the level of *Irakm* transcripts was measured over time. (**D**) Relative luciferase activity of pGL4-luc2 with WT-3′UTR (IRAKM-WT) or with IRAKM-3′UTR containing mutated m^{6}A sites (IRAKM-MUT) transfected into HEK293T cells was measured. The firefly luciferase activity was normalized to *Renilla* luciferase activity. Data are shown as representative results of three independent experiments (A) or as means ± SEM (B to D). $^{**}P < 0.01$ and $^{****}P < 0.0001$; NS, not significant (unpaired two-tailed Student's *t* test).

DISCUSSION

RBPs play a vital role in RNA metabolism, which is tightly connected to all aspects of cellular functions. However, the mechanisms by which RBP-mediated RNA regulation affects the activation of innate immune cells are largely unknown. Here, we have identified METTL3 as a positive regulator of the innate response of macrophages by using pooled RBP CRISPR-Cas9 screens. Specifically, we have demonstrated that METTL3-mediated m^{6}A modification of *Irakm* mRNA accelerates its degradation, resulting in reprogramming macrophages for activation. These findings provide a previously unappreciated mechanism for epitranscriptional control of innate response in macrophages. Nevertheless, we have not observed high-ranked individual m^{6}A readers in either TNF-α–Low or TNF-α–Hi cell population in our pooled RBP CRISPR-Cas9 screening. The functional redundancy of YTHDF proteins appears to exist in the innate immune response of macrophages (*33*, *34*), and our data show that the simultaneous knockdown of *Ythdf1*, *Ythdf2*, and *Ythdf3*, in contrast to knocking down each of these readers individually, can significantly reduce *Tnf*-α expression upon LPS stimulation.

Recent studies have shown that transcripts of key genes of the innate immune signaling pathway are marked by m^{6}A modifications, which are required for the maintenance of proper innate antiviral responses (*27*, *28*, *40*, *41*) or are essential for dendritic cell activation (*26*), indicating that the m^{6}A modification is implicated in innate immune responses. Our data document that *Mettl3* deficiency in macrophages reduces their proinflammatory cytokine production and thus suppresses their ability to defend against pathogens and eliminate tumors. Thus, the METTL3/m^{6}A modification appears to be required for macrophage activation–mediated innate immunity.

Activation of the TLR4 signaling and subsequent induction of effective positive feedback to augment immune response by proinflammatory cytokines has a pivotal role in eliminating invading pathogens. However, the magnitude of the immune response must be tightly regulated to avoid pathologic immune reactions. A previous study has shown that TLR4 activation could negatively regulate the stimulation of macrophages by inducing the expression of *Irakm* (*14*). Our data document that *Mettl3*-KO macrophages have a higher level of IRAKM expression than their WT counterparts, resulting in reduced TLR4 signaling. Except for TLR4 signaling, we observed that *Mettl3* deficiency could decrease TNF-α expression upon the activation of TLR3 or TLR9 signaling individually. These data support our previously proposed m^{6}A working model in which m^{6}A acts as a "gas pedal" specifically targeting immediate-early response genes, such as *Socs* in T cells and *Irakm* in macrophages, to trigger their rapid degradation and to ensure that the immune cells can quickly respond to the external stimuli and adapt to the environment (*24*). Later on, these cells increase the expression levels of

Socs or *Irakm* genes to "brake" the signaling by a feedback mechanism, thus preventing its overactivation.

The MeRIP-seq data demonstrated that *Irakm* transcripts were marked by m^{6}A modifications, removal of which retarded the degradation of *Irakm* mRNA, and the resulting excess of IRAKM protein blocked the TLR4 signaling. Thus, *Irakm* mRNA decay controlled by m^{6}A modification represents a novel mechanism of releasing the brake from the TLR4 signaling pathway. Consistently, our previous study showed that m^{6}A modification selectively targets the transcripts of the *SOCS* family genes, the "gatekeeper" of the IL-7/STAT5 signaling pathway, accelerating their degradation necessary to reprogram naive T cells for differentiation and proliferation (*24*). It was also demonstrated that IRAKM promotes lung tumor growth (*42*) and fibrosis in multiple organs (*15*, *43*) by skewing macrophage toward an alternative activated phenotype. *Mettl3*-deficient mice displayed enhanced tumor growth. TAMs and BMDMs from *Mettl3*$^{flox/flox}$;*Lyzm*-Cre mice polarized with either TCM or IL-4 exhibited elevated M2-related markers, suggesting that the balance of macrophage polarization was modulated at an epitranscriptional level by the m^{6}A modification of *Irakm* mRNA.

A recent study reported that the m^{6}A modification promotes dendritic cell activation by enhancing the translation of target transcripts, *CD40*, *CD80*, and *Tirap* (*26*). However, our MeRIP-seq data documented that *CD40* transcripts were not m^{6}A-marked, indicating that the targets of m^{6}A modification may be cell type specific. Moreover, the m^{6}A peaks of *CD80* and *Tirap* mRNA were not affected in *Mettl3*-deficient macrophages, suggesting the presence of additional unidentified m^{6}A writer (s) catalyzing the m^{6}A modification of *CD80* and *Tirap* transcripts in macrophages; such a possibility warrants further investigation.

The high ranking of m^{6}A writer genes in our CRISPR screening indicates the fundamental importance of m^{6}A regulation in macrophage activation. It has been recently reported that m^{6}A on carRNAs can globally tune chromatin state and transcription (*39*). However, neither did we observe a difference in chromatin openness and nascent RNA synthesis between BMDMs from *Mettl3*$^{flox/flox}$ mice and *Mettl3*$^{flox/flox}$;*Lyzm*-Cre mice, nor did we identify a significant m^{6}A peak on paRNA and eRNA upstream of *Tnf*-α and *Irakm*. Moreover, no significant carRNAs from TLR-related genes were identified. Therefore, in contrast to the observations in mESCs, our results demonstrated that in macrophages, m^{6}A regulates the levels of TNF-α posttranscriptionally, mostly by targeting the degradation of *Irakm* mRNA. In addition, we found that the m^{6}A levels of carRNAs for *Esrrb*, *Kmt2d*, and *LINE*, which have been proven to be decreased in Mettl3-KO mESCs, were not totally decreased in *Mettl3*-KO BMDMs (fig. S9). The difference in m^{6}A effects on chromatin status between METTL3-KO mESCs and METTL3-KO BMDMs may reflect differences in cellular contents and environmental context of stimuli-sensitive immune cells versus pluripotent ESCs (*21*, *34*).

In summary, our study demonstrates that m^{6}A modification represents a novel mechanism controlling the innate immune response of macrophages against environmental stimuli. In addition, the obtained results suggest that targeting m^{6}A modulators might be an effective therapeutic approach for inflammatory diseases and cancer.

MATERIALS AND METHODS

Mice

Mettl3$^{flox/flox}$ mice were generated as previously described (*24*) and crossed with *Lyzm*-Cre mice (the Jackson laboratory, Bar Harbor, ME, USA) to obtain CKO mice. The animals were maintained in specific pathogen–free facilities and used according to protocols approved by Animal Care and Use Committees of the Shanghai Jiao Tong University School of Medicine.

Infection

Age- and sex-matched *Mettl3*-WT and *Mettl3*-KO mice were infected orally with *S. typhimurium* strain ATCC 14028 at 10^8 bacteria per mouse. Body weights were monitored daily. Four days after infection, the bacterial burden in the spleen, liver, colon, and feces was determined by counting the colony-forming units (CFU) of the homogenized tissue on MacConkey agar plates.

Tumor model

MC38 murine colon adenocarcinoma cells were provided by Q. Zou, Shanghai Institute of Immunology of Shanghai Jiao Tong University, Shanghai. MC38 cancer cells were injected subcutaneously into 8-week-old female mice (5×10^5 cells per mouse). Tumor growth was measured as the tumor area.

Pooled CRISPR screening

For the pooled CRISPR screen, we designed 7272 sgRNAs targeting 782 RBPs using CRISPR-FOCUS (http://cistrome.org/crispr-focus/), listed in table S2. sgRNAs were cloned into lenti-puro-guide plasmid following an established protocol (*31*). Lenti-sgRNA constructs and packaging vectors (pMD2.G and psPAX2) were cotransfected into HEK293T cells, and virus-containing supernatant was collected. Cas9-expressing Raw 264.7 cells were infected with the lentiviral library at an infection rate of 30% and selected with puromycin. Seven days after selection, the infected cells were stimulated with LPS (100 ng/ml) plus brefeldin A for 6 hours and fixed and stained with phycoerythrin (PE)–conjugated TNF-α antibody for fluorescence-activated cell sorting.

High-throughput sequencing and bioinformatics analysis

The genomic DNA of cells collected just before sorting or sorted on the basis of TNF-α expression was isolated. The sgRNA library was barcoded and amplified with primers listed in table S3 for two rounds of PCR. Amplicons were purified and quantified for sequencing on Illumina HiSeq. The sequencing data generated from the screen and raw sgRNA counts have been submitted to the National Center for Biotechnology Information (NCBI) Database of Gene Expression Omnibus (GEO) Dataset under accession number GSE162469.

Dot blot assay

Total RNA from Raw 264.7 cells or BMDMs was extracted and enriched in mRNA with Dynabeads mRNA Purification Kit (Thermo Fisher Scientific, Ambion, 61006). mRNAs were then denatured at 95°C for 3 min and chilled on ice immediately. A 2-μl drop of mRNA was applied directly onto Amersham Hybond-N$^+$ membrane (GE Healthcare, RPN203B) and cross-linked to the membrane by Stratalinker 2400 UV Crosslinker. Unbounded mRNA was washed off with TBST [1× phosphate-buffered saline (PBS) supplemented with 0.02% Tween 20] for 5 min at room temperature and blocked with 5% nonfat milk in TBST for 1 hour at room temperature. The m^{6}A level was determined with an anti-m^{6}A antibody (Synaptic Systems, 202003).

Western blotting

Cells were collected and lysed on ice for 30 min in radioimmunoprecipitation assay buffer containing cocktails of protease

and phosphatase inhibitors, and the supernatants were subject to Western blot analysis.

Flow cytometry

BMDMs and Raw 264.7 cells were stimulated with LPS, IL-4, or TCM along with Golgi inhibitor for the indicated time. Then, single-cell suspensions were prepared from either cultured cells or tumor samples and incubated with antibody cocktails for 15 min at 4°C for cell surface staining. For intracellular cytokine staining, cells were fixed with BD Fixation/Permeabilization buffer (BD 554714) for 30 min at 4°C and subsequently stained with antibodies for 30 min at 4°C. Data were recorded on BD LSRFortessa X-20 and analyzed with FlowJo software.

Tumor-conditioned medium

MC38 cancer cells were cultured in Dulbecco's modified Eagle's medium (DMEM) supplemented with 10% fetal bovine serum (FBS) for 72 hours. The supernatant was collected, centrifuged, and stored at −80°C for further use.

Isolation and differentiation of BMDMs

Bone marrow cells were isolated from the hind leg femur of mice and differentiated into macrophages in DMEM supplemented with 10% FBS (Gibco) and 20% L929 cell culture supernatant for 7 days. Differentiated BMDMs were collected and replated in DMEM without the L929 cell culture supernatant for 12 hours and then stimulated with LPS (Sigma-Aldrich L2880, 10 ng/ml) and IL-4 (PeproTech 214-14-20, 25 ng/ml) for M1 and M2 polarization, respectively.

Plasmid construction and mutagenesis assays

pLVX-IRES-ZsGreen lentiviral vectors were a gift from Q. Zou (Shanghai Institute of Immunology, China). Lentiviruses encoding *Mettl3* and their mutants in pLVX-IRES-ZsGreen plasmids were produced in 293T cells, then collected, filtered through a 0.22-μm MCE membrane (Millipore), and used to infect BMDMs. MG-guide retrovirus vectors were a gift from R.A.F. (Department of Immunobiology, Yale University School of Medicine, USA). Retroviruses expressing specific shRNA targeting *Irakm* in MG-guide plasmids were produced and used to infect BMDMs as described above. The shRNA target *Irakm* transcripts are listed in table S3. The WT and m^{6}A motif disrupted 3′UTRs of *Irakm* were synthesized and cloned into MG-guide plasmids.

RNA interference

siRNAs targeting *Ythdf1*, *Ythdf2*, *Ythdf3*, and *Ythdc1* were transfected into BMDMs using Lipofectamine RNAiMAX (Invitrogen, Carlsbad, CA, USA) according to the manufacturer's instructions. The cells were analyzed 48 to 72 hours later. The siRNA sequences are listed in table S3.

DNase I–TUNEL experiment

The analysis of chromatin openness with DNase I–TUNEL assay was performed according to the method of Liu *et al.* (*39*). Briefly, BMDMs were permeabilized by 0.1% Triton X-100 in PBS for 10 min before digesting with DNase I (0.2 U/ml; New England Biolabs) and then fixed in 4% paraformaldehyde. Subsequently, the TUNEL assay (DeadEnd Fluorometric TUNEL System, Promega) was performed according to the manufacturer's instructions and followed by DAPI staining. Images were captured with an Olympus FV3000 confocal microscope, and the intensity of the nuclear TUNEL signal was quantified using ImageJ software.

Nascent RNA labeling assay

Nascent transcripts synthesis was analyzed according to the method of Liu *et al.* (*39*). Briefly, BMDMs were cultured on precoated cover glasses. A nascent RNA synthesis assay was conducted 24 hours later using the Click-iT RNA Imaging Kit (Invitrogen, C10329) according to the manufacturer's protocol. Images were captured with an Olympus FV3000 confocal microscope, and the intensity of the signal was quantified using ImageJ software.

Nascent RNA transcription rate measurement by qPCR

Nascent transcription rate was analyzed according to the method of Liu *et al.* (*39*). Briefly, BMDMs were seeded to the same amount of cells. After 48 hours, EU was added to 0.5 mM at 60, 30, 20, and 10 min before trypsinization collection. Total RNA was purified by TRIzol, and nascent RNA was captured by using Cell-Light EU Nascent RNA Capture Kit (RiboBio). RNA amount and EU adding time were fitted to a linear equation, and the slope was estimated as transcription rate of RNA.

Chromosome-associated RNA MeRIP-qPCR

The m^{6}A level of chromosome-associated RNAs was analyzed according to the method of Liu *et al.* (*39*). Briefly, total RNA was isolated from the chromosome-associated fraction of BMDMs, and nonribosomal RNA was further enriched by using Ribo-off rRNA Depletion Kit (human/mouse/rat; Vazyme). Fragmentation and MeRIP-qPCR were performed following the protocol in this paper.

Library preparation and Illumina HiSeq sequencing

RNA purification, reverse transcription, library construction, and sequencing were performed at WuXi NextCODE (Shanghai, China) according to the manufacturer's instructions (Illumina). Briefly, polyadenylated mRNA was purified from total RNA using oligo-dT–attached magnetic beads and fragmented by the fragmentation buffer. Taking these short fragments as templates, the first-strand cDNA was synthesized using reverse transcriptase and random primers, followed by the second-strand cDNA synthesis. The synthesized cDNA was subjected to end repair, phosphorylation, and "A" base addition, according to Illumina's library construction protocol. Next, Illumina sequencing adapters were added to both sides of the cDNA fragments. After PCR amplification for DNA enrichment, the target fragments of 200 to 300 base pairs (bp) were cleaned up.

After library construction, Qubit (Thermo Fisher Scientific) was used to quantify the concentration of the resulting sequencing libraries, while the size distribution was determined using the Agilent Bioanalyzer 2100 (Agilent). Then, the Illumina cBot cluster generation system with HiSeq PE Cluster Kits (Illumina) was used to generate clusters. Paired-end sequencing was performed at WuXi NextCODE (Shanghai, China) using an Illumina HiSeq system following the manufacturer's protocols for 2 × 150 paired-end sequencing. These RNA-seq data have been deposited on GEO public database under the accession number GSE162248.

MeRIP-qPCR and MeRIP-seq

Total RNA from WT or *Mettl3*-KO Raw 264.7 cells (with or without LPS stimulation) was extracted with the TRIzol reagent (Thermo Fisher Scientific, 15596018), and approximately 100 μg of total RNA for each condition was fragmented to ~100 bp in length with fragmentation buffer (10 mM tris-HCl and 10 mM $ZnCl_2$). The

RNA size after the fragmentation was validated by 2200 TapeStation detection (Agilent). A sample of 100 ng of the fragmented RNA was saved as the input control, while the remaining RNA was mixed with 50 μl of protein A magnetic beads (Thermo Fisher Scientific, 10002D) and 50 μl of protein G magnetic beads (Thermo Fisher Scientific, 10004D) premixed with 10 μg of anti-m^{6}A antibody (Merck Millipore, ABE572). The samples were incubated for 4 hours at 4°C in IP buffer [10 mM tris-HCl, 30 mM NaCl, and 0.1% (v/v) IGEPAL CA-630 supplemented with ribonuclease (RNase) inhibitor]. The beads were washed twice with 1× IP buffer, twice with low-salt IP buffer [50 mM NaCl, 10 mM tris-HCl (pH7.5), and 0.1% IGEPAL CA-630], and twice in 1000 μl of high-salt IP buffer [500 mM NaCl, 10 mM tris-HCl (pH7.5), and 0.1% IGEPAL CA-630]. RNA was eluted and purified with the RNeasy kit (QIAGEN) and eluted with 15-μl RNase-free water. Both input and enriched RNA samples were used for library preparation with TruSeq Stranded Total RNA Library Prep Human/Mouse/Rat (Illumina) according to the manufacturer's instructions.

For MeRIP-qPCR, approximately 1 μg of total RNA from WT or *Mettl3*-KO BMDMs was used. The input and enriched RNA were prepared using the same protocol as described above, but with scaled-down reagents, and dissolved in 10 μl of RNase-free water. The enrichment of m^{6}A was analyzed using the LightCycler 480. Myc peak and Myc body were used, respectively, as a positive and negative control for MeRIP-qPCR.

Analysis of m^{6}A RIP-seq

The raw reads were mapped to mouse ribosomal RNA sequences using bowtie2 to remove the reads that came from ribosomal RNA. The unmapped reads were then mapped to the mouse genome (GRCm38.p6 and gencode.vM20) using STAR. The potential bias caused by PCR amplification was removed using the Picard Mark Duplicates command. For m^{6}A-seq data, the fragment coverage of each base of all transcripts was calculated using custom script. The peak calling algorithm was modified from Ma *et al.* (*44*). To calculate the enrichment score, the average fragment coverage of the window was used instead of the read count. The m^{6}A level on carRNAs upstream of indicated genes was analyzed according to the method from Liu *et al.* (*39*). The m^{6}A RIP-seq data from this study have been deposited to GEO series GSE162254.

RNA degradation assay

BMDMs were seeded on 24-well plates with 1 million cells per well. Actinomycin D was added at a final concentration of 5 μM. Cells were collected (after 0, 0.5, 1, 2, and 3 hours), and total RNA was extracted for real-time qPCR. Data were normalized to the $t = 0$ time point.

Dual-luciferase assay

pGL4-luc2 (Firefly luciferase) vector of the Dual-Luciferase Reporter Assay System (Promega, E1910) was used to determine the function of m^{6}A modification within the 3′UTR of *Irakm* transcripts. The assay was performed according to the manufacture's instruction: Briefly, 100 ng of WT or m^{6}A-mutant IRAKM-3′UTR and 25 ng of pRL-TK (*Renilla* luciferase) control vector were cotransfected into HEK293T cells in triplicates. The relative luciferase activity was accessed 24 to 48 hours after transfection.

Statistical analysis

All data are presented as means ± SEM. Comparisons between groups were analyzed by the unpaired two-tailed Student's *t* test or two-way analysis of variance (ANOVA). Statistical analysis was performed using Prism 6 (GraphPad).

SUPPLEMENTARY MATERIALS

Supplementary material for this article is available at http://advances.sciencemag.org/cgi/content/full/7/18/eabd4742/DC1

View/request a protocol for this paper from *Bio-protocol*.

REFERENCES AND NOTES

1. T. Kawai, S. Akira, Toll-like receptors and their crosstalk with other innate receptors in infection and immunity. *Immunity* **34**, 637–650 (2011).
2. P. J. Murray, Macrophage polarization. *Annu. Rev. Physiol.* **79**, 541–566 (2017).
3. R. Noy, J. W. Pollard, Tumor-associated macrophages: From mechanisms to therapy. *Immunity* **41**, 49–61 (2014).
4. I. Vitale, G. Manic, L. M. Coussens, G. Kroemer, L. Galluzzi, Macrophages and metabolism in the tumor microenvironment. *Cell Metab.* **30**, 36–50 (2019).
5. D. G. DeNardo, B. Ruffell, Macrophages as regulators of tumour immunity and immunotherapy. *Nat. Rev. Immunol.* **19**, 369–382 (2019).
6. A. Mantovani, F. Marchesi, A. Malesci, L. Laghi, P. Allavena, Tumour-associated macrophages as treatment targets in oncology. *Nat. Rev. Clin. Oncol.* **14**, 399–416 (2017).
7. L. Cassetta, J. W. Pollard, Targeting macrophages: Therapeutic approaches in cancer. *Nat. Rev. Drug Discov.* **17**, 887–904 (2018).
8. T. Kawai, S. Akira, The role of pattern-recognition receptors in innate immunity: Update on Toll-like receptors. *Nat. Immunol.* **11**, 373–384 (2010).
9. D. N. Cook, D. S. Pisetsky, D. A. Schwartz, Toll-like receptors in the pathogenesis of human disease. *Nat. Immunol.* **5**, 975–979 (2004).
10. J. Su, T. Zhang, J. Tyson, L. Li, The interleukin-1 receptor-associated kinase M selectively inhibits the alternative, instead of the classical NFκB pathway. *J. Innate Immun.* **1**, 164–174 (2009).
11. D. Xu, H. Zhang, X. Wang, Y. Chen, Expression of IRAK-3 is associated with colitis-associated tumorigenesis in mice. *Mol. Med. Rep.* **16**, 3415–3420 (2017).
12. P. Fernandes, J. MacSharry, T. Darby, A. Fanning, F. Shanahan, A. Houston, E. Brint, Differential expression of key regulators of Toll-like receptors in ulcerative colitis and Crohn's disease: A role for Tollip and peroxisome proliferator-activated receptor gamma? *Clin. Exp. Immunol.* **183**, 358–368 (2016).
13. S. Gunaltay, N. Nyhlin, A. K. Kumawat, C. Tysk, J. Bohr, O. Hultgren, E. Hultgren Hornquist, Differential expression of interleukin-1/Toll-like receptor signaling regulators in microscopic and ulcerative colitis. *World J. Gastroenterol.* **20**, 12249–12259 (2014).
14. K. Kobayashi, L. D. Hernandez, J. E. Galan, C. A. Janeway Jr., R. Medzhitov, R. A. Flavell, IRAK-M is a negative regulator of Toll-like receptor signaling. *Cell* **110**, 191–202 (2002).
15. M. N. Ballinger, M. W. Newstead, X. Zeng, U. Bhan, X. M. Mo, S. L. Kunkel, B. B. Moore, R. Flavell, J. W. Christman, T. J. Standiford, IRAK-M promotes alternative macrophage activation and fibroproliferation in bleomycin-induced lung injury. *J. Immunol.* **194**, 1894–1904 (2015).
16. H. Zhou, M. Yu, K. Fukuda, J. Im, P. Yao, W. Cui, K. Bulek, J. Zepp, Y. Wan, T. W. Kim, W. Yin, V. Ma, J. Thomas, J. Gu, J. A. Wang, P. E. DiCorleto, P. L. Fox, J. Qin, X. Li, IRAK-M mediates Toll-like receptor/IL-1R-induced NFκB activation and cytokine production. *EMBO J.* **32**, 583–596 (2013).
17. J. C. Deng, G. Cheng, M. W. Newstead, X. Zeng, K. Kobayashi, R. A. Flavell, T. J. Standiford, Sepsis-induced suppression of lung innate immunity is mediated by IRAK-M. *J. Clin. Invest.* **116**, 2532–2542 (2006).
18. J. Tong, R. A. Flavell, H. B. Li, RNA m6A modification and its function in diseases. *Front. Med.* **12**, 481–489 (2018).
19. S. Zaccara, R. J. Ries, S. R. Jaffrey, Reading, writing and erasing mRNA methylation. *Nat. Rev. Mol. Cell Biol.* **20**, 608–624 (2019).
20. Y. Yang, P. J. Hsu, Y. S. Chen, Y. G. Yang, Dynamic transcriptomic m6A decoration: Writers, erasers, readers and functions in RNA metabolism. *Cell Res.* **28**, 616–624 (2018).
21. H. Shi, J. Wei, C. He, Where, when, and how: Context-dependent functions of RNA methylation writers, readers, and erasers. *Mol. Cell* **74**, 640–650 (2019).
22. G. Cao, H. B. Li, Z. Yin, R. A. Flavell, Recent advances in dynamic m6A RNA modification. *Open Biol.* **6**, 160003 (2016).
23. Z. Shulman, N. Stern-Ginossar, The RNA modification N6-methyladenosine as a novel regulator of the immune system. *Nat. Immunol.* **21**, 501–512 (2020).
24. H. B. Li, J. Tong, S. Zhu, P. J. Batista, E. E. Duffy, J. Zhao, W. Bailis, G. Cao, L. Kroehling, Y. Chen, G. Wang, J. P. Broughton, Y. G. Chen, Y. Kluger, M. D. Simon, H. Y. Chang, Z. Yin, R. A. Flavell, m6A mRNA methylation controls T cell homeostasis by targeting the IL-7/STAT5/SOCS pathways. *Nature* **548**, 338–342 (2017).
25. J. Tong, G. Cao, T. Zhang, E. Sefik, M. C. Amezcua Vesely, J. P. Broughton, S. Zhu, H. Li, B. Li, L. Chen, H. Y. Chang, B. Su, R. A. Flavell, H. B. Li, m6A mRNA methylation sustains Treg suppressive functions. *Cell Res.* **28**, 253–256 (2018).

26. H. Wang, X. Hu, M. Huang, J. Liu, Y. Gu, L. Ma, Q. Zhou, X. Cao, Mettl3-mediated mRNA m6A methylation promotes dendritic cell activation. *Nat. Commun.* **10**, 1898 (2019).
27. Y. Liu, Y. You, Z. Lu, J. Yang, P. Li, L. Liu, H. Xu, Y. Niu, X. Cao, N6-methyladenosine RNA modification-mediated cellular metabolism rewiring inhibits viral replication. *Science* **365**, 1171–1176 (2019).
28. Q. Zheng, J. Hou, Y. Zhou, Z. Li, X. Cao, The RNA helicase DDX46 inhibits innate immunity by entrapping m6A-demethylated antiviral transcripts in the nucleus. *Nat. Immunol.* **18**, 1094–1103 (2017).
29. Y. Zhang, X. Wang, X. Zhang, J. Wang, Y. Ma, L. Zhang, X. Cao, RNA-binding protein YTHDF3 suppresses interferon-dependent antiviral responses by promoting FOXO3 translation. *Proc. Natl. Acad. Sci. U.S.A.* **116**, 976–981 (2019).
30. D. Han, J. Liu, C. Chen, L. Dong, Y. Liu, R. Chang, X. Huang, Y. Liu, J. Wang, U. Dougherty, M. B. Bissonnette, B. Shen, R. R. Weichselbaum, M. M. Xu, C. He, Anti-tumour immunity controlled through mRNA m6A methylation and YTHDF1 in dendritic cells. *Nature* **566**, 270–274 (2019).
31. J. Joung, S. Konermann, J. S. Gootenberg, O. O. Abudayyeh, R. J. Platt, M. D. Brigham, N. E. Sanjana, F. Zhang, Genome-scale CRISPR-Cas9 knockout and transcriptional activation screening. *Nat. Protoc.* **12**, 828–863 (2017).
32. O. Parnas, M. Jovanovic, T. M. Eisenhaure, R. H. Herbst, A. Dixit, C. J. Ye, D. Przybylski, R. J. Platt, I. Tirosh, N. E. Sanjana, O. Shalem, R. Satija, R. Raychowdhury, P. Mertins, S. A. Carr, F. Zhang, N. Hacohen, A. Regev, A genome-wide CRISPR screen in primary immune cells to dissect regulatory networks. *Cell* **162**, 675–686 (2015).
33. S. Zaccara, S. R. Jaffrey, A unified model for the function of YTHDF proteins in regulating m6A-modified mRNA. *Cell* **181**, 1582–1595.e18 (2020).
34. L. Lasman, V. Krupalnik, S. Viukov, N. Mor, A. Aguilera-Castrejon, D. Schneir, J. Bayerl, O. Mizrahi, S. Peles, S. Tawil, S. Sathe, A. Nachshon, T. Shani, M. Zerbib, I. Kilimnik, S. Aigner, A. Shankar, J. R. Mueller, S. Schwartz, N. Stern-Ginossar, G. W. Yeo, S. Geula, N. Novershtern, J. H. Hanna, Context-dependent functional compensation between Ythdf m^{6}A reader proteins. *Genes Dev.* **34**, 1373–1391 (2020).
35. A. P. West, A. A. Koblansky, S. Ghosh, Recognition and signaling by Toll-like receptors. *Annu. Rev. Cell Dev. Biol.* **22**, 409–437 (2006).
36. B. S. Zhao, I. A. Roundtree, C. He, Post-transcriptional gene regulation by mRNA modifications. *Nat. Rev. Mol. Cell Biol.* **18**, 31–42 (2017).
37. J. Y. Roignant, M. Soller, m^{6}A in mRNA: An ancient mechanism for fine-tuning gene expression. *Trends Gen.* **33**, 380–390 (2017).
38. Y. Lee, J. Choe, O. H. Park, Y. K. Kim, Molecular mechanisms driving mRNA degradation by m^{6}A modification. *Trends Gen.* **36**, 177–188 (2020).
39. J. Liu, X. Dou, C. Chen, C. Chen, C. Liu, M. M. Xu, S. Zhao, B. Shen, Y. Gao, D. Han, C. He, N6-methyladenosine of chromosome-associated regulatory RNA regulates chromatin state and transcription. *Science* **367**, 580–586 (2020).
40. L. Wang, M. Wen, X. Cao, Nuclear hnRNPA2B1 initiates and amplifies the innate immune response to DNA viruses. *Science* **365**, eaav0758 (2019).
41. R. Winkler, E. Gillis, L. Lasman, M. Safra, S. Geula, C. Soyris, A. Nachshon, J. Tai-Schmiedel, N. Friedman, V. T. K. Le-Trilling, M. Trilling, M. Mandelboim, J. H. Hanna, S. Schwartz, N. Stern-Ginossar, m^{6}A modification controls the innate immune response to infection by targeting type I interferons. *Nat. Immunol.* **20**, 173–182 (2019).
42. T. J. Standiford, R. Kuick, U. Bhan, J. Chen, M. Newstead, V. G. Keshamouni, TGF-β-induced IRAK-M expression in tumor-associated macrophages regulates lung tumor growth. *Oncogene* **30**, 2475–2484 (2011).
43. S. Steiger, S. V. Kumar, M. Honarpisheh, G. Lorenz, R. Gunthner, S. Romoli, R. Grobmayr, H. E. Susanti, J. Potempa, J. Koziel, M. Lech, Immunomodulatory molecule IRAK-M balances macrophage polarization and determines macrophage responses during renal fibrosis. *J. Immunol.* **199**, 1440–1452 (2017).
44. L. J. Ma, B. X. Zhao, K. Chen, A. Thomas, J. H. Tuteja, X. He, C. He, K. P. White, Evolution of transcript modification by N^6-methyladenosine in primates. *Genome Res.* **27**, 385–392 (2017).

Acknowledgments: We thank M. Yang, S. Hu, Y. Zhou, and all other members of the Hua-Bing Li laboratory for discussions and comments. **Funding:** This work was supported by the National Natural Science Foundation of China (91753141/82030042/32070917 to H.-B.L., 81822021/91842105 to S.Z., 81801550 to J.T., and 81901580 to Y.L.), the Shanghai Science and Technology Committee (grant no. 20JC1417400/201409005500/20JC1410100 to H.-B.L.), the Program for Professor of Special Appointment (Eastern Scholar) at Shanghai Institutions of Higher Learning (to H.-B.L.), the start-up fund from the Shanghai Jiao Tong University School of Medicine (to H.-B.L.), the National Key R&D Program of China (2018YFA0508000) (to S.Z.), the Strategic Priority Research Program of the Chinese Academy of Sciences (XDB29030101) (to S.Z.), and the Howard Hughes Medical Institute (to R.A.F.). **Author contributions:** H.-B.L. conceived the project and designed the research. J.T., X.W., and Y.L. designed and performed the murine portion of the study. H.-B.L., J.T., and X.W. analyzed and interpreted the data and wrote the manuscript. X.R., A.W., and S.Z. performed and analyzed the bacterial infection model. Y.L. and J.Y. generated *Mettl3*-deficient Raw 264.7 cells, and Y.L., J.Y., and K.M. helped with experiments involving Raw 264.7 cells. Q.Z. provided MC38 cells. Z.C. and Y.Z. helped with analyzing RNA-seq data. W.P., Q.Z., Y.Z., Q.X., J.L., S.Z., R.A.F., and H.-B.L. discussed the projects. This study was supervised by H.-B.L. and R.A.F. All authors read and approved the final manuscript. **Competing interests:** R.A.F. is a consultant for GSK and Zai Lab Ltd. All other authors declare that they have no competing interests. **Data and materials availability:** All data needed to evaluate the conclusions in the paper are present in the paper and/or the Supplementary Materials. Sequenced reads have been deposited in the NCBI GEO database (accession nos. GSE162254, GSE162248, and GSE162469). Additional data related to this paper may be requested from the authors.

Submitted 23 June 2020
Accepted 8 March 2021
Published 28 April 2021
10.1126/sciadv.abd4742

Citation: J. Tong, X. Wang, Y. Liu, X. Ren, A. Wang, Z. Chen, J. Yao, K. Mao, T. Liu, F.-L. Meng, W. Pan, Q. Zou, J. Liu, Y. Zhou, Q. Xia, R. A. Flavell, S. Zhu, H.-B. Li, Pooled CRISPR screening identifies m^{6}A as a positive regulator of macrophage activation. *Sci. Adv.* **7**, eabd4742 (2021).

Pooled CRISPR screening identifies m^{6}A as a positive regulator of macrophage activation

Jiyu Tong, Xuefei Wang, Yongbo Liu, Xingxing Ren, Anmin Wang, Zonggui Chen, Jiameng Yao, Kaiqiong Mao, Tingting Liu, Fei-Long Meng, Wen Pan, Qiang Zou, Jun Liu, Yu Zhou, Qiang Xia, Richard A. Flavell, Shu Zhu and Hua-Bing Li

Sci Adv **7** (18), eabd4742.
DOI: 10.1126/sciadv.abd4742